

ASSESSMENT OF THERMALLY ACTUATED PUMPING IN AN OPEN-ENDED CHANNEL WITH MULTI-SCALE SURFACE ASYMMETRY

Ramuel Safarkoolan¹, Emre Ozen¹, Vinod Narayanan^{1*}, Sushil Bhavnani²

¹University of California, Davis, CA

²Auburn University, Auburn, AL

ABSTRACT

Passive fluid pumping during boiling using the concept of asymmetry in the geometry of the heated surface is studied experimentally. The geometry consists of a channel that is located within a chamber filled with dielectric fluid. The channel ends (inlet and outlet) are exposed to the chamber, such that the ends of the channel have the same pressure prior to the addition of heat. Two types of asymmetry are introduced on the heated surface, and their effect is assessed on the net bubble growth and motion within the open-ended channel. The first is a millimeter-scale asymmetry caused by contouring the vertical walls of the channel into repeating 60-30-degree ratchets. The second asymmetry consists of microscale reentrant cavities, located periodically on the shallow ratchet face of the ratchet. To assess the motion of two-phase flow within the channel, visualization at various heat fluxes ranging from 0.8 – 2.6 W/cm² and subcooling from 2.7 - 11.5 °C is performed. Videos of bubble ebullition, mergers and slug transport are analyzed to obtain growth rates, velocities, and frequency counts of slugs emanating from either end of the open-ended channel.

Keywords: asymmetry, thermal pumping, boiling, ratchets, thermal management

NOMENCLATURE

q''	heat flux (W/cm ²)
T_{pool}	pool fluid temperature (°C)
T_{sat}	fluid saturation temperature based on pressure (°C)

1. INTRODUCTION

Passively-driven thermal loops based on boiling heat transfer in the evaporator have been studied for several decades. Various configurations of such loops driven by gravitational [1, 2], inertial [3, 4], or capillary forces [5] have been developed in the past. In this study, thermally-actuated fluid motion driven by asymmetry in surface geometry is discussed.

Use of asymmetry in driving liquid motion in a preferential direction in the evaporator has been explored in the literature in different formats. Lin and Prosperetti [3] used asymmetry in the location of a periodically actuated microheater in a capillary tube connecting two reservoirs to drive the liquid from one reservoir to the other. Linke et al. [6] discovered that droplets placed on heated surface with periodic mm-scale asymmetry resulted in propulsion in a preferential direction in the Leidenfrost regime. Ok et al. [7] found that reducing the size of the ratchets resulted in greater speed of droplet over the heated surface. Kapsenberg et al. [8] studied pool boiling from a vertically upward facing asymmetric surface such as that developed by Linke et al [6]. In addition to the asymmetry of the periodically repeating ratchet surface, they added a second asymmetry by locating cavities on the shallow face of the ratchets. They found that bubbles departed normal to the shallow face. A simple force balance model was put forth to determine the net horizontal velocity impacted by the growing droplet on the ratchet face. Experiments and the model predicted liquid velocity horizontal to the surface in the order of 20 mm/s. Thiagarajan et al. [9] performed pool boiling microgravity experiments with a similar test section and found that the vapor bubbles moved horizontally along the heated surface, in a manner very similar to what Linke et al. found with liquid droplets in the Leidenfrost regime.

In this paper, bubble motion in an open-ended channel comprised of vertically-oriented heated surfaces with ratchets and preferentially-oriented cavities is experimentally characterized.

* Direct all the comments/concerns to the corresponding author at: vnarayanan@ucdavis.edu

In prior work [10], the bubble motion within such an open-ended channel with one level of asymmetry- in the form of mm-scale ratchets with 60-30-degree angle, was studied. Directional motion of slugs in open-ended channels was observed, and a phenomenological model of slug motion based on a Couette-Poiseuille flow in the thin film between the vapor slug and the ratchet walls was proposed. The addition of the second asymmetry in the form of preferentially-located cavities, brings about another potential mechanism for propulsion of the two-phase flow - that of momentum transfer by the growing bubble to the surrounding fluid. The goal is to determine the net effect of the multi-tier asymmetries on the two-phase flow within the open-ended channel. As a step towards this goal, image analysis of bubble motion for various heat flux and subcooling conditions for a mm-scale ratchet test section is described in this work. The eventual goal is to develop a closed-loop, passive, thermally-actuated device with such an evaporator for high heat flux cooling applications.

2. MATERIALS AND METHODS

The details of the ratchet test section with two levels of asymmetry is first discussed, followed by the test chamber and procedure.

2.1 Ratchet test sections

Figure 1A shows a drawing of the ratchet test section design that were fabricated using wire electric discharge machining (EDM). The angles on the ratchet faces were 30 - 60 degrees and the pitch in the design shown in Fig. 1.a was 3.0 mm. Slot cavities with a reentrant design were located in every third ratchet on the shallow slope. The crest and trough of the ratchets were rounded to prevent stray nucleation sites at these locations. On the heated side, two notches 250 μm wide, and 2 mm deep were designed on each ratchet to mitigate axial heat conduction.

Figure 1.b shows an exploded view of the open-ended channel. The top and bottom walls were made of clear polycarbonate while the vertical ratchet walls of the channel were made of grade 5 titanium. The ratchet test sections spanned 70 mm. Thick-film heaters that spanned 18 mm in length and 4 mm in depth were located on the backside of the ratchet test section and located in between the two notches. Each heater was composed of a 0.254 mm thick steel serpentine shim, and sealed within Kapton tape. High-temperature Ultem™ plastic was used to insulate the backside of the heaters. By controlling the voltage applied to the serpentine heaters, precise control of the heat flux through the titanium ratchet was achieved.

2.2. Test chamber

The experimental test chamber is shown in Fig. 2. The chamber consisted of a polycarbonate base and top, sandwiched by an aluminum chamber. The side walls of the aluminum chamber is equipped with an internal fluidic channel to provide for temperature control of the pool. The experimental chamber was placed on four legs with adjustable heights to enable precise

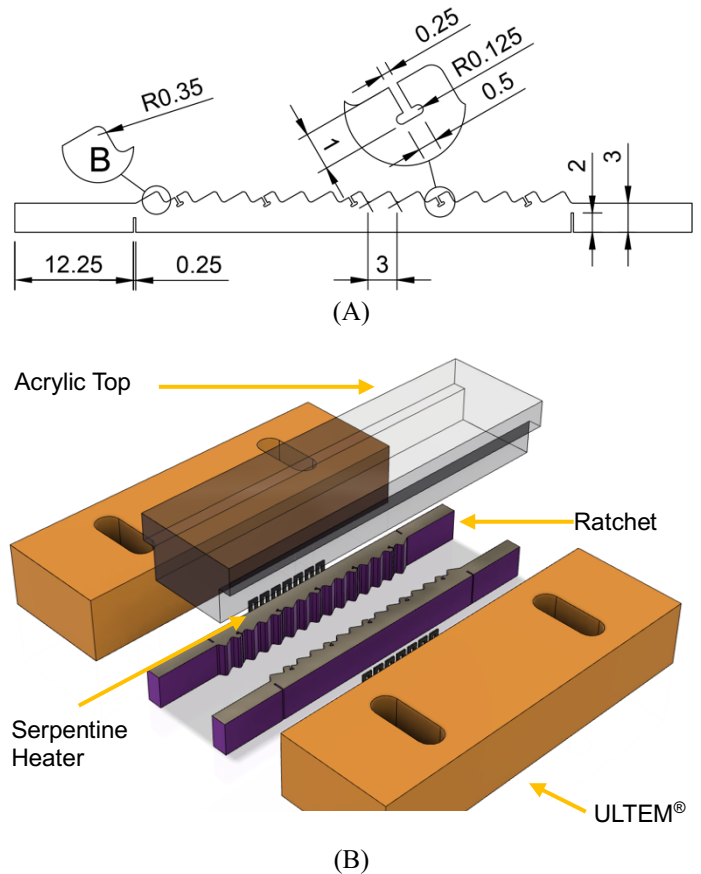


Figure 1. (a) fabricated 60-30 degree ratchet test section dimensions. All dimensions are in mm. (b) exploded view of the open ended channel with vertical walls

leveling. Thermocouples were inserted through the top polycarbonate lid to read pool temperature and vapor temperature. A pressure transducer was used to record chamber pressure. The aluminum side wall with fluidic channel was exposed both to the pool and the vapor, controlling both the pool temperature, vapor temperature, and chamber pressure through condensation. For additional condensation control, a copper condensation loop was provided within the chamber. Desired subcooling values at stable chamber pressures could be achieved through coupled tuning of the aluminum fluidic loop temperature and copper condensation loop flow rate.

Each ratchet, heater and Ultem insulating block were assembled individually and placed at the center of the chamber. A clear precision polycarbonate block was used to position the walls parallel to each other. After securing the walls to the chamber, the polycarbonate piece was used as an upper wall spanning the gap between the two vertical walls. Fluid was in communication with the pool in the chamber through the two channel ends. The copper condensation loop was in contact only with the vapor, and not the liquid. When assembled, viewed from the front the channel had a height equal to the thickness of the heated ratchets, 6.35 mm, and a width of 9 mm.

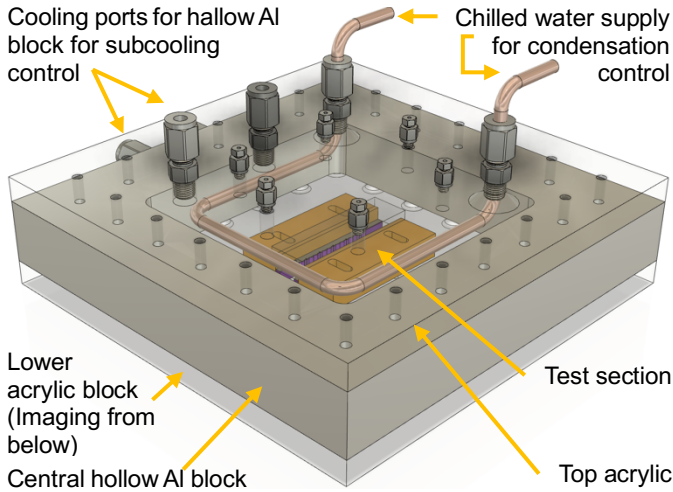


Figure 2. Exploded view of the test chamber; the ratchets shown in Fig. 1 form the vertical walls of the open channel at the center of the chamber

2.3. Experimental procedure

To eliminate the effects of the gravity on the experiment, the channel was leveled carefully. The leveling was performed using a standing bubble test described herein. At low subcooling and heat flux, a bubble was generated inside the channel by turning on the ratchet heaters. At the onset of departure of a vapor bubble from the vertical ratchet surface, the power to the heaters was turned off. The legs on which the experimental setup stood were adjusted until the generated bubble remained stationary for a period of 2 minutes. To further ensure that gravity did not have an effect on results, for one condition, the chamber was rotated 180 degrees around an axis perpendicular to the largest face of the chamber, and the standing bubble test and adjustment was repeated. Tests for a similar heat flux and subcooling were performed in this 180 degree rotated orientation as the 0 degree orientation.

Preliminary experiments were performed to determine the range of stable subcooling and heat flux permitted by the experimental facility. The limits were set at conditions in which nucleation was beginning to occur on the low end, and at conditions in which slugs were continuously visible in the channel, at the high end. These experiments helped form an operational map, shown in Fig. 3, for further experiments. The chamber was filled with dielectric fluid (FC-72) and a vacuum was pulled to remove air from the chamber as well as to degas the fluid. Next, the heaters were powered to achieve the selected heat flux on the operational map. The temperature of the aluminum loop was controlled using a circulation chiller. If the aluminum loop alone could not provide sufficient condensation to maintain a stable chamber pressure, the copper condenser loop was further used. It should be noted that heat flux was determined using the rectangular surface area of the heater (2.4 cm²).

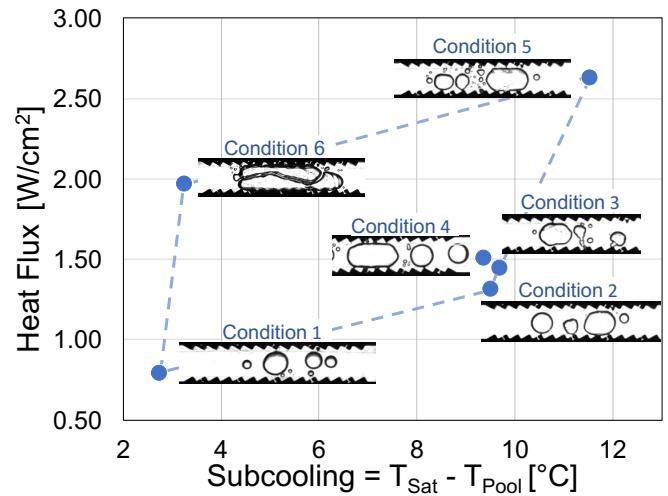


Figure 3. Operational map and representative images at select steady state conditions

3. RESULTS AND DISCUSSION

Qualitative visualization results from several test conditions shown in Fig. 3 are first shown followed by quantitative results from image processing. In the discussion of videos, a slug is defined as a bubble with length larger than the channel width. All of the video sequences were captured at 50 frames per second and spanned 90 s. A lower frame rate was chosen so that multiple slug departures from the channel could be recorded for statistical analysis.

Table 1. Summary of test conditions

Cond.	Heat Flux [W/cm ²]	Subcooling [°C]	T _{pool} [°C]	T _{vapor} [°C]
1	0.79	2.73	11.3	11.7
2	1.31	9.50	27.5	28.6
3	1.45	9.70	29.7	32.3
4	1.51	9.36	26.7	26.6
5	2.63	11.5	31.2	30.9
6	1.97	3.26	11.8	13.9

Table 1 summarizes the test conditions which spanned from 0.8 to 2.63 W/cm² of heat flux and 1.89 to 9.70 (°C) of subcooling.

3.1. Qualitative visualization

To validate the accuracy of the standing bubble leveling procedure, experiments with similar conditions (3 and 4 in Table 1, and Fig.3) were performed.

Figure 4 shows a sequence of images from the recorded videos. For ease of comparison sequence of images from 0 degree orientation conditions 3 (figure 4.A), and the 180 degree

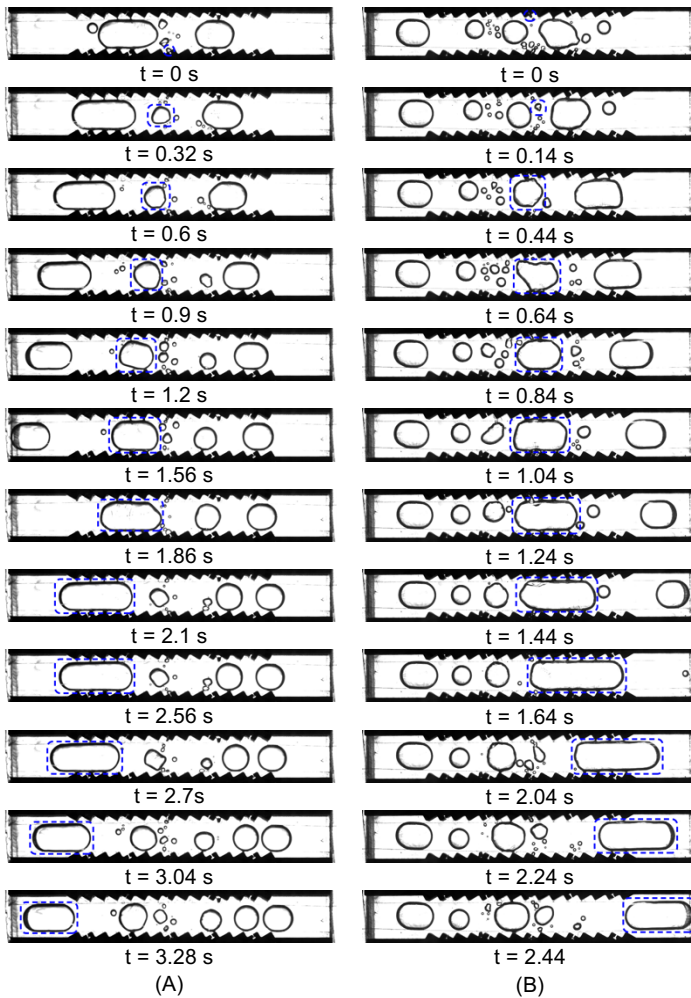


Figure 4. Effect of orientation on pumping phenomenon- Side by side sequence of images from visualization of similar test conditions 3.a 4.b. For ease of viewing, for each conditions a sample bubble life cycle is highlighted by the blue dashed area

orientation condition 4 (figure 4.b), are presented side by side. The sequence depicts the life cycle of a typical bubble (see dotted blue line identifying the bubble under consideration), as it departs from the slot cavities on the shallow slope of the ratchet wall and forms a slug by merging with other bubbles. In both of these conditions, bubbles which depart from the shallow face in the central heated region of the channel coalesce to form a larger slug. The slug expands along the lateral direction rapidly and grows under the impact of smaller bubbles from the shallow face. When the slug is no longer moving due to coalescing, it still grows by the addition of heat from the heated ratchets through the thin liquid film. This growth continues until the slug reaches the non-heated part of ratchet, $t = 2.56$ s for A, and $t = 1.64$ s for B. The slug then condenses and contracts in size, and departs the channel. The period from inception to draining for the studied bubble in condition 3 was 3.28 s, while the period for the bubble for condition 4 was 2.44 s. This discrepancy in period is attributed to the slightly higher heat flux and lower subcooling of condition 4 compared with condition 3 (see Table 1).

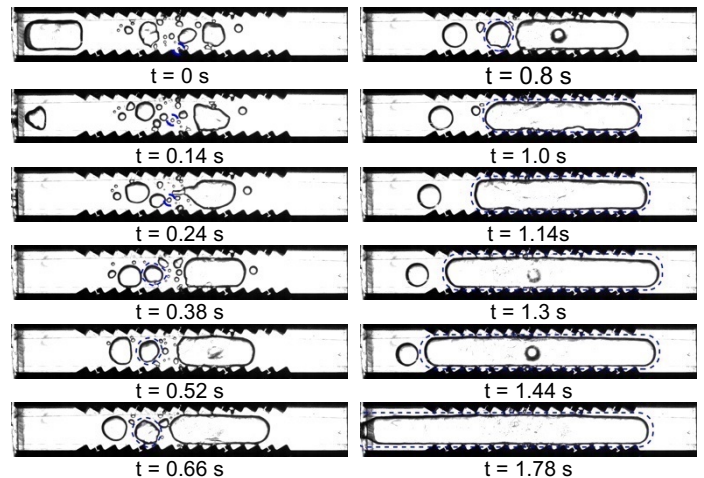


Figure 5. Sequence of images from visualization; subcooling: 11.5 °C; heat flux: 2.63 W/cm². For ease of viewing, a sample bubble life cycle is highlighted by the blue dashed area

Fig. 5 shows a sequence of images from the recorded video at test condition 5 with 11.5 °C subcooling and a heat flux of 7.2 W/cm². This condition corresponds to the highest heat flux and subcooling tested (see Fig. 3). The sequence depicts the life cycle of a typical bubble (see dotted line identifying the bubble under consideration), as it progresses from departure from the slot cavity at the shallow ratchet wall to the formation of a slug by coalescence with other bubbles. At this high sub-cooling and high heat flux condition, bubbles that depart from the shallow face in the central heated region of the channel coalesce to form a larger slug that encompasses the entire length of the ratchet walls. The slug expands along the lateral direction rapidly and grows under the impact of smaller bubbles from the shallow face. The sequence from $t = 0.8$ s to $t = 1.78$ s shows that the extent of the bubble is larger towards the left end than the right end, and the slug eventually departs the left end of the channel.

Fig. 6 shows and life cycle of a typical slug at the second test condition. At this high sub-cooling and low heat flux condition, the life cycle of a typical slug (at ~6.5 s) was considerably longer than the high flux condition shown in Fig. 5 (~1.8 s). The growth and departure of isolated bubbles from the central slot cavity in the shallow face of the ratchet is clearly visible in this sequence of images ($t = 0$ s to $t = 0.94$ s). The bubbles merge with a larger slug upon departure ($t = 2.26$ s) and the horizontal momentum imparted on the larger slug seems to propel the slug to the left ($t = 4.38 - 5.4$ s) and the slug departs from the left side of the channel at $t = 6.5$ s.

Fig. 7 shows the life cycle of a typical slug for the first test condition shown in Table 1. At this low heat flux and low subcooling condition, the life cycle (at ~3s) is about twice the period of the higher subcooling and high heat flux condition 5 (Fig. 5), but about one half that of the low heat flux and high subcooling in condition 2 (Fig. 6). As in the sequence shown in Fig. 7, the bubble emerging from the ratchet at $t = 0.7$ s merges with a larger bubble at $t = 1.14$ s. This larger bubble then

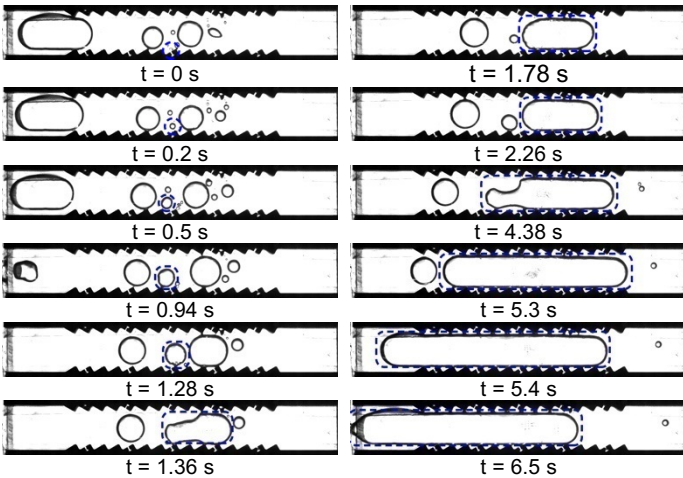


Figure 6. Visualization sequence of images from the second experimental condition; subcooling: 9.5 °C; heat flux: 1.31 W/cm². For ease of viewing, a sample bubble life cycle is highlighted by the blue dashed area

merges with a slug to the right. The slug eventually departs to the right side at $t = 3.04$ s.

The lowest subcooling and high heat flux in condition 6 resulted in rapid slug growth (Fig. 3, top left image). The slugs grew and exited from both sides of the test section without exhibiting any discernable preferential motion.

3.2. Image Analysis

In order to extract quantitative results from the video sequence shown in Figs. 4-6, a modified version of an image-processing MATLAB[®] program developed by the group [11] was used. This program resolved the area, major-axis length, minor-axis-length, and velocity of each bubble in each given image frame. The bubble edges were identified using two types of edge detection filters: a Laplace filter, and a Sobel filter. By using multiple filters, it was possible to identify bubbles that any one filter may have otherwise missed. Since there was no distinct edge for bubbles/slugs that were in contact with the ratcheted elements, a baseline image without bubbles in the channel was subtracted from the image sequence to be processed. The resulting subtracted image contained only bubble information with some noise. To improve the quality of image analysis the entire subtracted image was once and the channel area was 50 times processed with a 3x3 median filter. After filtering to identify bubbles, the image was binarized using an adjustable binarization threshold, and bubbles were filled. A conversion factor from pixels to mm was obtained through calibration with the known ratchet dimensions. By matching bubbles in one frame to the nearest bubble in the next frame, the respective velocities of the bubbles were calculated.

A 3x3 Laplace operator, and a 2x2 Sobel area were used in the video sequence corresponding to Fig. 5 with binarization thresholds of 0.15, and 0.15, respectively.

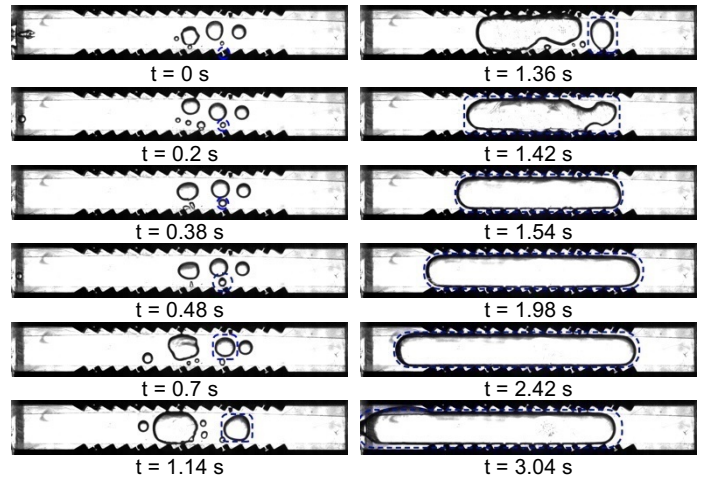


Figure 7. Sequence of visualization of images from condition 1; subcooling: 2.7 °C; heat flux: 0.79 W/cm². For ease of viewing, a sample bubble life cycle is highlighted by the blue dashed area

The life cycle of multiple slugs such as those shown in Figs. 4-7 were analyzed over the duration of recording to provide statistical information on directional motion at their corresponding test condition.

Fig. 8 correspond to processed data of area and speed over life cycle of a typical bubble for test condition 3 in Fig. 4. Since the image processing program requires an edge to resolve information from the bubble, Fig. 8 only show information before the leading edge of the slug departs the field of view.

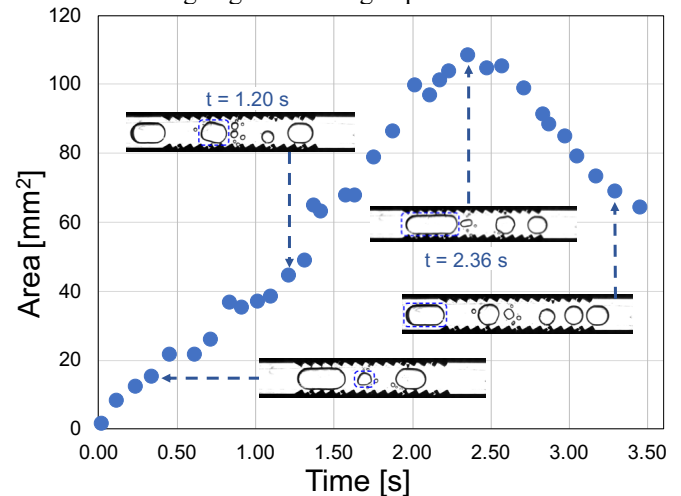


Figure 8. Area over slug life cycle for test condition 3.

From Fig. 8 three phases of bubble growth are observed. In the initial 1.2 seconds, the small bubble that emanates from the shallow slope of the ratchet departs the ratchet and coalesces with other bubbles departing from that location at later times to form a larger bubble with time. At around $t = 1.2$ s, the bubble spans the width of the channel to the crests of the ratchets. The newly formed slug now grows in size not only by absorbing smaller bubbles, but also by receiving heat from the heated

ratchet. This second phase represents the slug growth with area increase occurring only along the length of the channel until the slug reaches its largest size at $t = 2.36$ s. Beyond this point the slug passes over the unheated section of the ratchet and condenses, thereby reducing its size prior to departure from the channel through the right side. The slug continues to condense until it leaves the channel at ~ 3.5 s.

Statistical information on direction of bubble motion, length of slugs at departure, and frequency of departure of slugs was obtained by analyzing the entire video recording (for example, 93 seconds for condition 3). All departing bubble lengths (major-axis length) from either end of the open channel for each condition were analyzed and shown in the histogram in Fig. 9. The preferential direction for slug motion due to momentum imparted of the small bubbles is along the shallow slope of the ratchets from the steep side. In Fig. 9, blue bars indicate slugs departing from the preferential direction, while orange bars denote the slug motion along the steep side from the shallow side, and eventual departure from the right end of the open channel. Using the aforementioned image detection algorithm, the major axis size of the slugs just before their departure was measured. In order to determine the slug length at departure, an average of six consecutive frames prior to departure were used. From Fig. 9.a it is observed that for the condition of low heat flux and low subcooling, all slugs during the recording period depart from the preferential direction with a mean length of 60-62 mm.

For the condition of low heat flux and high subcooling, Fig. 9.b indicates that only slugs which are larger than 49 mm are departing in the preferential direction, while the bubbles departing from the adverse direction are smaller than 7 mm. Although the number of adverse departures, at 6, is substantial compared to that of the slugs departing from the preferential direction, at 10, when the departure length is considered it is obvious that more vapor flows out of the preferential direction. This condition exhibited the lowest number of preferential slug departures, due to the high subcooling and low heat flux.

The third and fourth test conditions corresponded to medium heat flux and high subcooling. Recall that conditions 3 and 4 were similar in their subcooling and applied heat flux, but the chamber was rotated 180 degree relative to the other. This rotation required replication of the experiment by readjusting the chamber. For the third condition (0 degree rotation), Fig. 9.c, preferential bubble/slug departure ranged from 5.2 mm to 55.6 mm. About half of the preferential departures are due to bubbles (<9 mm), while the rest of the departures are attributed to slugs. The length of the departed adverse bubble/slugs ranged from 6 mm to 15 mm. Among all test conditions, this condition showed the highest number of adverse bubble departures with a total count of 7 which is 1 count lower than that of either of the conditions before or after it. In the fourth condition (180 degree rotation), as depicted in Fig. 9.d, 12 bubbles and 32 slugs are observed to depart from the preferential direction. A total of 5 bubbles, and only one slug depart from the adverse direction.

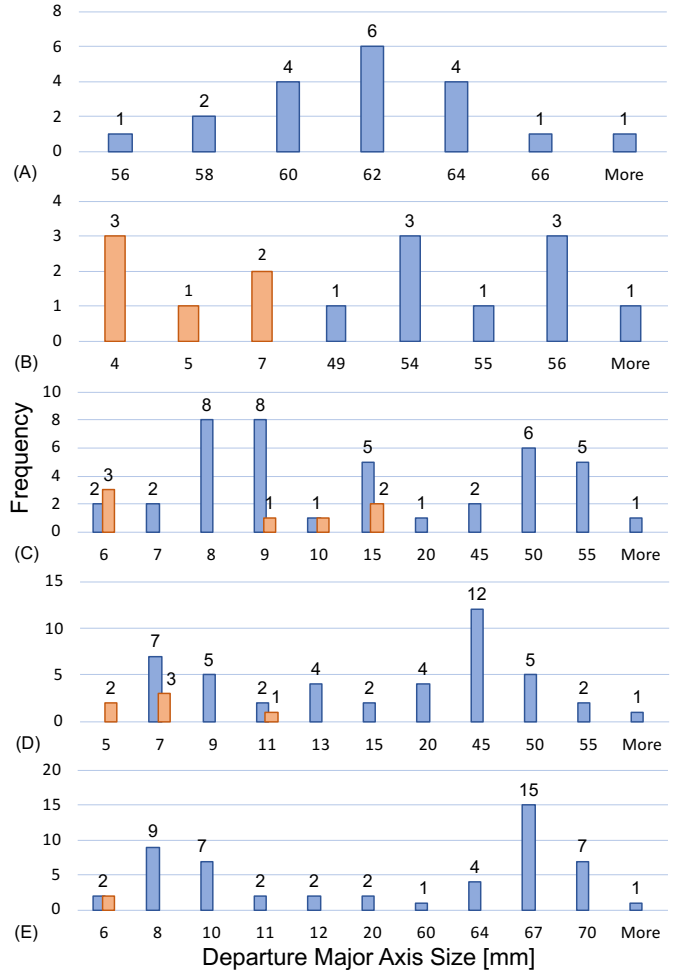


Figure 9. Histogram of bubbles/slugs of each length departing channel. Blue bars correspond to departures in the preferential direction, while orange ones correspond to departures in the adverse direction. Panels a-e map to test conditions 1-5 respectively (see Table 1 for conditions).

A total of 7 and 6 stray departures were observed for condition 3 and 4, respectively. Comparing the count of adverse departures for the two conditions, it can be concluded that the standing bubble leveling method was effective in eliminating the influence of gravity on directional motion of bubbles and slugs. The highest heat flux and high subcooling condition 5 (Fig. 9.e) not only had the most slugs/bubbles departure count, but also the largest departing slug of 71.5 mm of all the test conditions. In this condition, only two bubbles of sizes up to 6 mm departed in the adverse direction. Fig. 9.e shows that the length distribution of the preferential bubble departure is bimodal with means of 6-8 mm, and 64-67 mm.

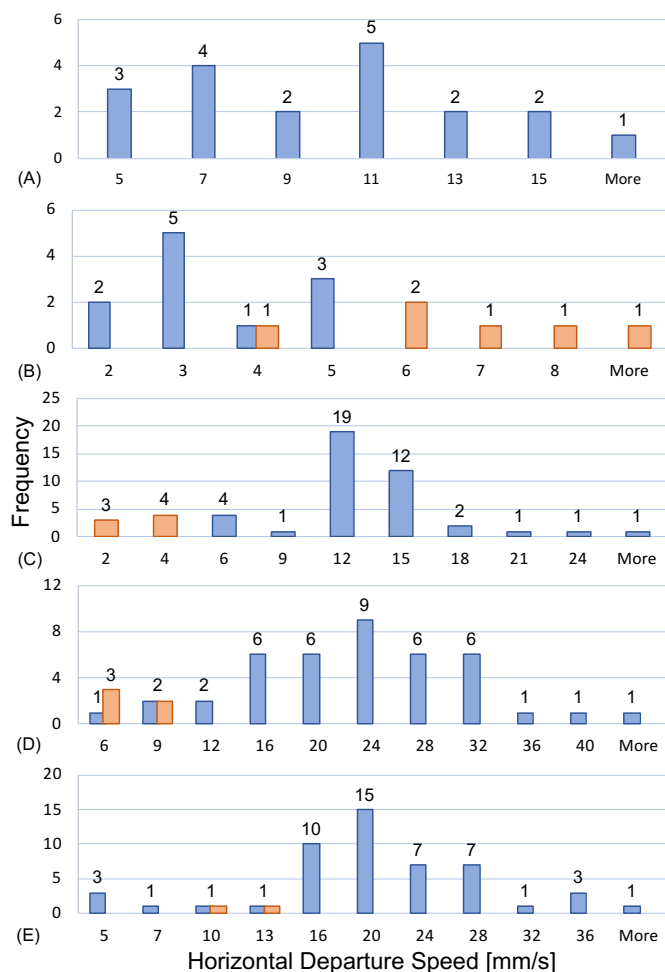


Figure 10. Histogram of bubbles/slugs of each horizontal speed departing channel. Blue bars correspond to departures in the preferential direction, while orange ones correspond to departures in the adverse direction. Panels a-e map to conditions 1-5 respectively in Table 1.

Analysis similar to that performed to obtain the departing length was also used to calculate the horizontal speed of bubbles/slugs at departure, hence forth referred to as departure speed. The x centroid of a slug/bubble for two consecutive frames was used to calculate each departure speed. As with the departure slug length, an average of speed estimated from up to six consecutive frames was used to provide a better representation of the departure speed. The results of such analysis for all of the bubbles, and conditions are presented in Fig. 10.

For the first condition, whose results are shown in Fig 10.a, departures occurred in the preferential direction with a minimum 3.73 mm/s, and a maximum departure speed of 15.5 mm/s. As evident from Fig. 10.a majority of the departures happened with a departure speed range of 9-11 mm/s.

The fastest recorded preferential departure for the second condition, was 4.53 mm/s, and the fastest adverse departure

¹ To improve the statistical representation of the distribution, for this data set a single outlier data was removed.

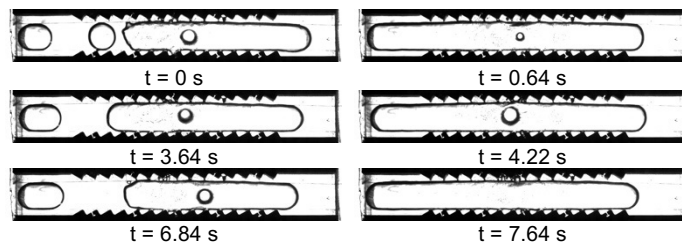


Figure 11. Selected frames from condition 5, depicting bubble departure frequency for the shorter slug (left panel) and longer slug (right panel).

speed (albeit for bubbles and not slugs) was 8.77 mm/s. As depicted in Fig 10.b slugs with speeds in the range of 2-3 mm/s had the most number of the preferential departures (5).

Unlike the second case, in which most adverse departures were faster than all of the preferential direction, all of the preferential departures left the channel faster than all of adverse departures Fig. 10.c. For this condition the 9-12 mm/s preferential departure speed interval had the most (19) number of bubbles. For the test condition case 4, from Fig. 10.d it is observed that the preferential departure is a normal distribution with an average around the 20-24 mm/s range. The fastest stray departure was at most 9 mm/s.

Similar to the fourth condition, the departure speed of condition 5 was a normal distribution with an average around the 16-24 mm/s, Fig. 10.e. There were only two adverse departures recorded for this condition ranging from 10-13 mm/s. Out of the studied conditions, condition 5 had the fastest stray departure speed, which is to be expected given the high heat flux at this condition.

TABLE 2. SUMMARY OF ANALYSIS

Cond.	Total Bubble Count	Preferential Volumetric Flow Rate [mm ³ /s]	Adverse Volumetric Flow Rate [mm ³ /s]	Preferential Bubble Departure Frequency [Hz]
1	19	1120	0	0.23±0.019 (19)
2	15	468	9	0.10±0.0072 (9)
3	48	747	29	0.30±0.13 (17); 1.00±0.33 (23)
4	50	961	16	0.41± 0.12 (30); 1.61± 0.64 (12) ¹
5	54	1780	4	0.34± 0.023 (25); 0.69±0.34 (27)

Based on the departure number and volume, the volumetric flow rate of vapor was computed and is reported in Table 2. To obtain the volume of each bubble, results from image processing of major and minor axis of each bubble/slug was used along with the assumption that the ends of the bubbles were perfect

hemispheres and that the bubbles were cylindrical. The total volume was then divided by the duration of the video sequence in each case to arrive at a vapor volumetric flow rate.

Comparing conditions 1 and 2, it is seen that an increase in subcooling has a negative effect on volumetric flow rate. This comparison becomes more prominent when the first case is compared to either the fourth, or the third case. While the heat flux for the fourth case is almost twice that of the first case, the volumetric flow in the fourth case is still lower than that of the first case. Comparing cases 2-5, it is seen that an increase in heat flux results in a substantial increase in the volumetric flow rate, despite the higher subcooling of condition 5.

The average slug departure frequency is shown in the last column of Table 2. The numbers in the parenthesis are the number of data points used to calculate the departure frequency. While slugs in conditions 1-2 departed with a fixed frequency, the slugs in the conditions 3-5 departed with two distinct dominant frequencies. For the latter cases it was observed that, for most part, shortly after the departure of a smaller slug, Fig. 11 top left, a larger slug would follow, Fig. 11 top right. Merging with all the bubbles and slugs in its path, the large slug depletes the channel of any vapor, creating a large time gap until the next departure, Fig. 11 middle left.

4. CONCLUSIONS

An experimental study of two-phase flow motion generated by use of multi-scale asymmetry in the heated surface is performed in an open-ended channel configuration. The heated walls consisted of mm-scale asymmetry in the form of repeating 60-30 degree ratchets and sub-mm scale reentrant slots, periodically located on the shallow face of the ratchets. Visualization was performed over a range of heat fluxes from 0.8 - 2.6 W/cm² and subcooling in the range of 2.7 - 11.5 °C. Salient results are summarized below:

- Bubbles emerged, grew, and departed from the reentrant cavities normal to the shallow face
- At the lower heat flux bounds and under all tested subcooling conditions (Fig. 3), bubbles departing the shallow face of the ratchets were seen to impact the larger slugs and bubbles within the channel at an angle normal to the shallow face. This impact was seen to further propel the larger bubbles and slugs in a preferential direction in the channel along the shallow face of the ratchet.
- For all of the conditions directional propulsion of bubbles and slugs was observed using multi-level asymmetry.
- A decrease in subcooling and an increase in heat flux increased the volume of the vapor leaving the channel.

ACKNOWLEDGEMENTS

Financial assistance for the project provided by NSF under Grant 1740515 and 1740506 is gratefully acknowledged. The authors thank Mr. Hoai Nguyen for assistance with the chamber fabrication and initial experimentation.

REFERENCES

- [1] Mukherjee S., Mudawar I., "Smart Pumpless Loop for Micro-Channel Electronic Cooling Using Flat and Enhanced Surfaces", IEEE Transaction on Components and Packaging Technologies, Vol. 26, No. 1, March 2003.
- [2] Kuo S., Shih C., Chang C., Chen S., "Bubble pump in a closed-loop system for electronic cooling", Applied Thermal Engineering 51 (2013), pp. 425-434.
- [3] Torniainen E. D., Govyadinov A. N., Markel D. P., Komilovitch P. E., "Bubble-driven inertial micropump", Physics of Fluids 24, 2012, p. 122003.
- [4] Yin Z., Prosperetti A., "Blinking bubble' micropump with microfabricated heaters", Journal of Micromechanics and Microengineering 15 (2005), pp. 1683-1691.
- [5] Peterson, G. P., 1994, *An Introduction to Heat Pipes-Modeling, Testing, and Applications*, First edition, Wiley Interscience, New York.
- [6] Linke H., Alemán B. J., Melling L. D., Taormina M. J., Francis M. J., Dow-Hygelund C. C., Narayanan V., Taylor R. P., and Stout A., "Self-Propelled Leidenfrost Droplets." Physical Review Letters. 96 (15), p. 154502.
- [7] Ok, J. T., Lopez-Oña, E., Nikitopoulos, D. E., Wong, H., and Park, S., 2011, "Propulsion of droplets on micro- and sub-micron ratchet surfaces in the Leidenfrost temperature regime," Vol. 10(5), pp. 1045-1054.
- [8] Kapsenberg, F., Strid, L., Thiagarajan, N., Narayanan, V., and Bhavnani, S. H., 2014, "On the Lateral Fluid Motion During Pool Boiling via Preferentially Located Cavities," Applied Physics Letters, Vol. 104, 154105 (2014); doi: 10.1063/1.4871863.
- [9] Thiagarajan, N., Bhavnani, S. H., and Narayanan, V., 2015, "Self-Propelled Sliding Bubble Motion Induced by Surface Micro-Structure in Pool Boiling of a Dielectric Fluid under Microgravity," ASME Journal of Electronics Packaging, Vol. 137 (2), 021009 (8 pages)
- [10] Bhavnani, S. H., Thiagarajan, N., Narayanan, V., and Strid, L., 2019, "Passive directional motion of fluid during boiling driven by surface asymmetry in a dielectric fluid," Journal of Enhanced Heat transfer, Vol 26(4), pp. 393-413.
- [11] Kapsenberg, F., 2011, "Lateral fluid motion in nucleate boiling through asymmetric surface structures," M.S. Thesis, Oregon State University, Corvallis, OR, USA, 2011.